Size-Dependence of the Enhanced Raman Scattering of Pyridine Adsorbed on Ag_n ($n = 2-8, 20$) Clusters

Lasse Jensen,* Lin Lin Zhao, and George C. Schatz

Department of Chemistry, Northwestern University, 2145 Sheridan Road, Evanston, Illinois 60208-3113

Received: November 16, 2006; In Final Form: January 8, 2007

We present a time-dependent density functional theory (TDDFT) study of the size-dependence of the absorption and Raman scattering properties of pyridine interacting with small silver nanoclusters Ag_n ($n = 2-8, 20$). By employing a recently developed short-time approximation for the Raman scattering cross section we simulate both the normal and the "surface"-enhanced Raman spectra. The absorption spectra of the small silver clusters are studied both in the gas phase and embedded in rare gas matrices. We find that both the absorption and Raman properties depend strongly on cluster size and adsorption site. The normal Raman spectra of Ag_n−pyridine complexes resemble that of isolated pyridine, with enhancements which increase as cluster size increases. In contrast to this, both the enhancement and the appearance of the "surface"-enhanced Raman spectrum show a very strong dependence on cluster size. The total enhancements for the complexes are between 10^3 and 10^4 and quite surprisingly the strongest enhancement is found for the Ag_2−Py complex. However, the enhancement trends can be correlated with the distance of the molecule to the center of the metal cluster and with the resonance polarizability in a way that is suggestive of electromagnetic enhancements, so the enhancement mechanism for these small clusters is similar to what is found for larger particles.

I. Introduction

The optical properties of noble metal nanoparticles have long been of great technological and fundamental interest. The most important characteristics of these nanoparticles is that they exhibit collective oscillations of the conduction electrons known as *surface plasmons*. Excitation of plamons by light at a wavelength where resonance occurs leads to broad and size-/shape-dependent plasmon absorption bands in the UV−visible region. In addition, a strongly enhanced electromagnetic field is produced near the nanoparticle surface that is responsible for the electromagnetic contribution to the intense Raman signals observed in surface-enhanced Raman scattering (SERS).[1−4] Control of these optical properties has resulted in a wide range of applications in ultrasensitive chemical and biological sensing.[3,5−7]

A great deal of progress has been made recently in the accurate and efficient calculation of nanostructure optical properties. Although metallic nanoparticles are well described by using classical electrodynamics, deviations occur when the particle sizes become smaller than ∼10 nm.[4,8−11] As the particle size decreases further to only a few atoms, the classical description is no longer valid since the particle shows molecular-like electronic structure due to its low density of states. First-principles modeling combined with available experimental spectroscopic data provides a better description of the electronic structure and optical properties of clusters of different size.[4,10−13]

While it is mainly the absorption and emission properties of particles that have been studied, the Raman scattering properties of small clusters have also attracted attention.[14−16] The combination of resonance Raman spectroscopy and first-principles calculations has provided detailed information about cluster structure. Recently Dickson et al.[17] have shown that small (2−8 atom) silver clusters encapsulated in a dendrimer or peptide scaffold can produce single-molecule Raman scattering characteristic of the scaffold. This result is quite surprising since single molecule Raman has only been observed for molecules adsorbed onto large nanoparticles (>30 nm) in past work, where the strongly enhanced local field near the nanoparticle surface due to plasmon excitation is expected to be operative.[18−21]

It is generally believed that one or several of the following four contributions are needed to produce huge SERS enhancements for molecules adsorbed on small clusters: (a) strong enhancement due to ground state chemical interactions between molecule and cluster that are not associated with resonance excitations of the cluster−molecule system; (b) standard resonance Raman enhancement with the excitation wavelength being resonant with a molecular transition; (c) charge-transfer (CT) resonance Raman enhancement with the excitation wavelength being resonant with cluster−molecule CT transitions; and (d) enhancement in which the excitation wavelength is resonant with the strong excitations in the metal cluster (the analogue to plasmon excitation in larger nanoparticles). For molecules adsorbed on larger nanoparticles, the first three contributions are often grouped together as the "chemical mechanism" and the last is the "electromagnetic mechanism".[2,22,23] However, a complete picture of the enhancement mechanism for a given system, in particular, how individual contributions and their relative importance vary as a function of the cluster size, is not yet available.

In this paper, we present first-principles studies of the size-dependence of absorption and enhanced Raman scattering for a molecule adsorbed on small (atomic) silver clusters. In our previous works,[24,25] we have developed a Time-Dependent Density Functional Theory (TDDFT) method to calculate both on- and off-resonant Raman scattering, based on a short-time approximation to the Raman scattering cross section. We have applied this approach to study the absorption and Raman

* Address correspondence to this author. E-mail: l.jensen@chem.northwestern.edu.

10.1021/jp067634y CCC: $37.00
Published on Web 03/07/2007

scattering of the Ag_{20}−pyridine[26] and Ag_{20}−pyridazine−Ag_{20} model systems.[27] The results indicate that the absorption properties of a 20 atom silver tetrahedral cluster behave quite similarly to plasmon excitation observed in nanoparticles, and the Raman enhancement due to this cluster is comparable to findings on larger nanoparticles (>10 nm), at least as far as the traditional SERS enhancement is concerned. In this paper we extend the application of this TDDFT approach to study Ag_n−pyridine model systems with $n = 2-8$. This extension allows for a detailed systematic investigation of the absorption and enhanced Raman scattering of pyridine interacting with silver clusters of different size.

In addition, we present theoretical results on the effect of a rare gas matrix on the absorption spectra of these small clusters. Neutral or charged small silver clusters (≤8) show strong visible fluorescence,[28−33] and they have generally been studied in an embedding rare gas matrix that prevents photofragmentation and allows for the absorption signal to be measured.[28,29] Although the perturbation due to these matrices is thought to be small, it does cause the absorption spectrum to red-shift and broaden.[34] To model this matrix effect, we have used the COnductor-like Screening MOdel of solvation (COSMO) model,[35,36] as implemented in TDDFT,[37] to simulate absorption spectra of the clusters embedded in a dielectric medium.

II. Computational Details

Absolute Raman intensities are presented here in terms of the differential Raman scattering cross section. For Stokes scattering with an experimental setup having a 90° scattering angle and perpendicular plane-polarized light, the cross section is given by[38]

$$\frac{d\sigma}{d\Omega} = \frac{\pi^2}{\epsilon_0^2}(\tilde{\nu}_{in} - \tilde{\nu}_p)^4 \frac{h}{8\pi^2 c\tilde{\nu}_p}[45\bar{\alpha}_p'^2 + 7\gamma_p'^2] \times \frac{1}{45[1 - \exp(-hc\tilde{\nu}_p/k_B T)]} \quad (1)$$

where $\tilde{\nu}_{in}$ and $\tilde{\nu}_p$ are the frequency of the incident light and of the p'th vibrational mode, respectively. $\bar{\alpha}_p'$ and γ_p' are the isotropic and anisotropic polarizability derivatives with respect to vibrational mode p. The electronic polarizabilities both on- and off-resonance have been calculated by including a finite excited-state lifetime in the TDDFT calculation.[24,25] This finite lifetime is included phenomenologically by a common damping parameter Γ,[39−42] which describes relaxation and dephasing of the excited state. Values of Γ are related to the absorption line shape and the resonance Raman excitation profile, and can be estimated from the experimental absorption spectra (if available). However, one should realize that there is also a contribution arising from the solvent if the data correspond to a molecule in the condensed phase.[41,42] For small silver clusters embedded in rare gas matrices, the typical widths are about 0.2 eV[34] and a common damping parameter is therefore chosen to be $\Gamma = 0.1$ eV (corresponds to half the width). Note that this value is also what we found to be reasonable in earlier studies.[24−27,43]

All calculations presented in this work have been done by using a local version of the Amsterdam Density Functional (ADF) program package.[44,45] The Becke−Perdew (BP86) XC-potential[46,47] and a triple-ζ polarized Slater-type (TZP) basis set from the ADF basis set library have been used. A full electron basis set has been used for N, C, and H whereas the 1s−3d core has been frozen for Ag. Scalar relativistic effects have been accounted for by means of the zeroth-order regular approximation (ZORA).[48,49] The vibrational frequencies and normal modes have been calculated within the harmonic approximation. We have shown previously that the BP86 functional gives harmonic frequencies of pyridine close to experimental results without the use of scaling factors.[26]

The effects of rare gas matrix and water (when included) are investigated with use of the COSMO[35,36] approach, using a recent implementation[37] within ADF. This new code now includes the dynamic response of the solvent due to the perturbing electric field, and the nonequilibrium solvation response that is important for calculation of the response properties. Three different solvent parameters are needed in the calculations: the effective radius R_{solv}, which can be derived from the macroscopic density and molecular mass; the optical dielectric constant, ϵ_{op}, which is related to the refractive index; and the static dielectric constant, ϵ_{st}. For the solvents used in this work we adopted the following parameters: argon ($\epsilon_{st} = \epsilon_{op} = 1.66$, and $R_{solv} = 1.88$ Å), krypton ($\epsilon_{st} = \epsilon_{op} = 1.88$, and $R_{solv} = 2.00$ Å), xenon ($\epsilon_{st} = \epsilon_{op} = 2.22$, and $R_{solv} = 2.18$ Å), and water ($\epsilon_{st} = 78.5$, $\epsilon_{op} = 1.78$, and $R_{solv} = 1.9$ Å). For the rare gases only equilibrium properties are presented since the optical and static dielectric constant are identical. In addition, a van der Waals radius for each atom is needed to build the solvent cavity. The values used are the following: Ag, 2.025 Å; H, 1.35 Å; C, 1.700 Å; and N, 1.608 Å. Different values for the empirical factor scaling of the COSMO model were tested, with the default value giving the best results.

III. Results and Discussion

A. Geometry. As mentioned earlier, many experimental and theoretical studies have been done to address the structural, electronic, and optical properties of small silver clusters. Theoretically, Bonačić-Koutecký et al.[50,51] have used coupled cluster methods to determine the structure and absorption spectra of small Ag_n clusters ($n \leq 9$). Yabana and Bertsch,[52] and later Jellinek et al.,[53] have used TDDFT within the local density approximation (TDLDA) approach to calculate the optical properties of Ag_n clusters ($n \leq 8$). The most stable structures obtained from these studies were found to have the same topologies as the corresponding sodium clusters, and the structures of Ag_n are planar up to $n = 6$.[50,51,53] For larger clusters there exist many local minima close in energy, and the global minimum might not be the spectroscopically relevant configuration due to matrix or temperature effects. This is illustrated by the Ag_8 cluster, where a T_d and a D_{2d} structure were found to be very close in energy, with the T_d structure as the global minimum while the absorption spectrum of the D_{2d} structure is in better agreement with experiment.[51] However, a distorted T_d structure due to matrix interactions could also explain the observed spectrum.

In this work, we adopt the most stable structures found in ref 53: a linear Ag_2 ($D_{\infty h}$), a planar Ag_4 (D_{2h}), a planar trapezoidal Ag_6 (D_{3h}), and a distorted bicapped octahedron Ag_8 (T_d). The structure of the Ag_{20} cluster is the same as our previous work: a tetrahedral pyramidal T_d.[26] The structures optimized by using the BP86 xc-functional are found to have slightly longer bond lengths than those of Bonačić-Koutecký et al.[50,51] but are in good agreement with those given in ref 53. The absorption of pyridine onto a silver surface can occur either through the π electron, i.e., lying flat on the surface, or through the lone pair of the nitrogen, i.e., standing upright on the surface.[54−58] The exact absorption geometry depends on many factors such as coverage, temperature, substrate, and the electrochemical potential.[54−58] The most direct and recent

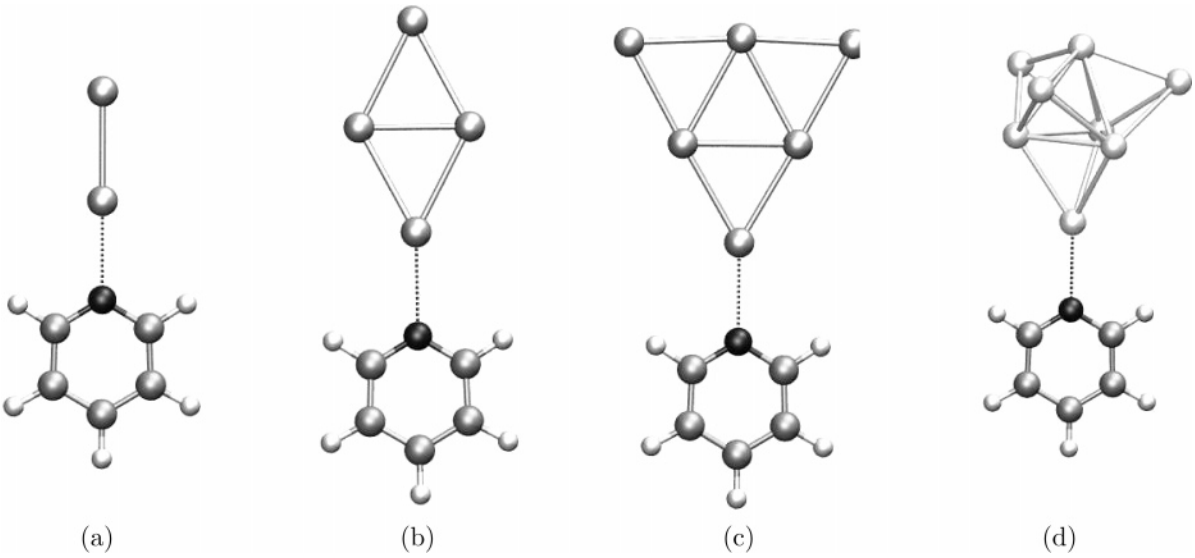

Figure 1. Optimized geometries for the Ag_n−Py ($n = 2-8$) complexes.

TABLE 1: Binding Interactions between Pyridine and the Ag_n ($n = 2-8$, 20) Clusters[a]

	R(Ag−N)	q(Py→Ag)	ΔE^{bind}
Ag_2−Py	2.261	0.136	−14.4
Ag_4−Py	2.380	0.149	−7.17
Ag_6−Py	2.301	0.148	−12.31
Ag_8−Py	2.308	0.148	−11.76
Ag_{20}−Py (VERT)	2.299	0.157	−13.02
Ag_{20}−Py (SURF)	2.459	0.132	−5.21

[a] Bond length between N and Ag atoms, R(Ag−N) in angstroms; ground state charge transfer between pyridine and cluster, q(Py→Ag) in units of electron charge; and total binding energy, ΔE^{bind} in kcal/mol.

evidence for the absorption geometry comes from low-temperature scanning tunneling microscope (STM) experiments by Hahn and Ho.[58] The STM image is consistent with pyridine standing upright on the surface, indicating that it binds through its nitrogen lone pair. Other evidence that pyridine binds through its N atom on silver surfaces is the observation of a vibrational band around 239 cm^{-1} in SERS experiments.[59−61] This band is usually assigned to a Ag−N bond stretch since this lies in the range of frequencies (200−287 cm^{-1}) found for metal−ligand stretching in many different N-bonded metal−pyridine complexes.[62] Such an assignment is also supported by enhanced Raman spectra for matrix-isolated Ag_n−pyridine ($n = 1-3$) complexes, which show a band at ∼242 cm^{-1} that is not found in pure matrix-isolated Ag_n samples.[61] We will therefore also assume such an absorption geometry in this work and the optimized Ag_n−pyridine ($n = 2-8$) complexes, denoted as Ag_n−Py, are as illustrated in Figure 1. The orientation of the pyridine molecule with respect to the clusters is so that it retains the ring-symmetry plane of pyridine. Furthermore, we assume that the structures of the silver clusters in the complexes are similar to those of the free clusters. Although it is possible that the complexes do not correspond to the global minima, we will not consider this any further, due to the rather weak interactions between the closed-shell silver clusters and the pyridine molecule.

The binding interactions between pyridine and the Ag_n ($n = 2-8$, 20) clusters are presented in Table 1. The two Ag_{20}−Py complexes have configurations (not shown) similar to the results published before,[26] but with shorter bond lengths and accordingly stronger binding energies (due to inclusion of relativistic effects). Basis set superposition errors are not corrected here since they were found previously to be rather small (<1 kcal/mol) for the two Ag_{20}−Py complexes.[26] For all the systems studied here, we see that forming a Ag_n−Py complex leads to partial charge transfer from the pyridine molecule to the silver cluster. Except for the Ag_4−Py and Ag_{20}−Py (SURF) complexes, binding energies between pyridine and the Ag_n cluster are around −12 kcal/mol, which is in good agreement with the desorption energy of 11.8 kcal/mol reported experimentally for a monolayer of pyridine on a Ag(111) surface.[63] The longer Ag−N bond lengths and lower binding energies for the Ag_4−Py and Ag_{20}−Py (SURF) complexes show that they do not correspond to their most favorable adsorption configurations. In fact, it is more favorable for pyridine to adsorb on the short axis of the Ag_4 cluster (rather than the long axis adopted here), and on the vertex of the Ag_{20} cluster (the VERT configuration). This shows that the absorption site of pyridine onto the silver cluster is more important than the cluster size in determining their binding interactions.

TABLE 2: Lowest Excitation Energies for the Ag_n ($n = 2-8$, 20) Clusters

	TDDFT/gas	TDDFT/Ar	TDLDA[a]	CCSD[b]	exptl/Ar[c]
Ag_2	3.06	2.87		2.94	2.80
Ag_4	2.97	2.75	3.01	3.21	3.07
Ag_6	2.42/3.23	2.43/3.06	∼2.5/∼3.2	3.06/3.69	
Ag_8	3.03/3.97	2.91/3.83	3.02/3.82	3.27/4.16	3.16/3.89
Ag_{20}	3.28	3.14			3.70

[a] Reference 53. [b] References 50 and 51. [c] References 31 and 34.

B. Absorption Spectra. The most important lowest energy excitations for the Ag_n ($n = 2-8$, 20) clusters are listed in Table 2, together with previous TDLDA,[53] CCSD,[50,51] and experimental results.[31,34] We see that our DFT results are in good agreement with the previous TDLDA results, but are somewhat lower than the CCSD results. Compared with the experimental results, we see that our COSMO-TDDFT approach underestimates the excitation energy, in particular, for the Ag_{20} cluster. One possible explanation could be a different conformer of Ag_{20}, since DFT studies[64,65] predict that the T_d structure of Ag_{20} is not the lowest minimum in the gas phase. However, we cannot rule out other explanations like shortcomings of the DFT functional, basis set, COSMO model, or a combination of these effects.

The simulated absorption spectra of the Ag_n ($n = 2-8$, 20) clusters in the gas phase and Ar, Kr, and Xe matrices are

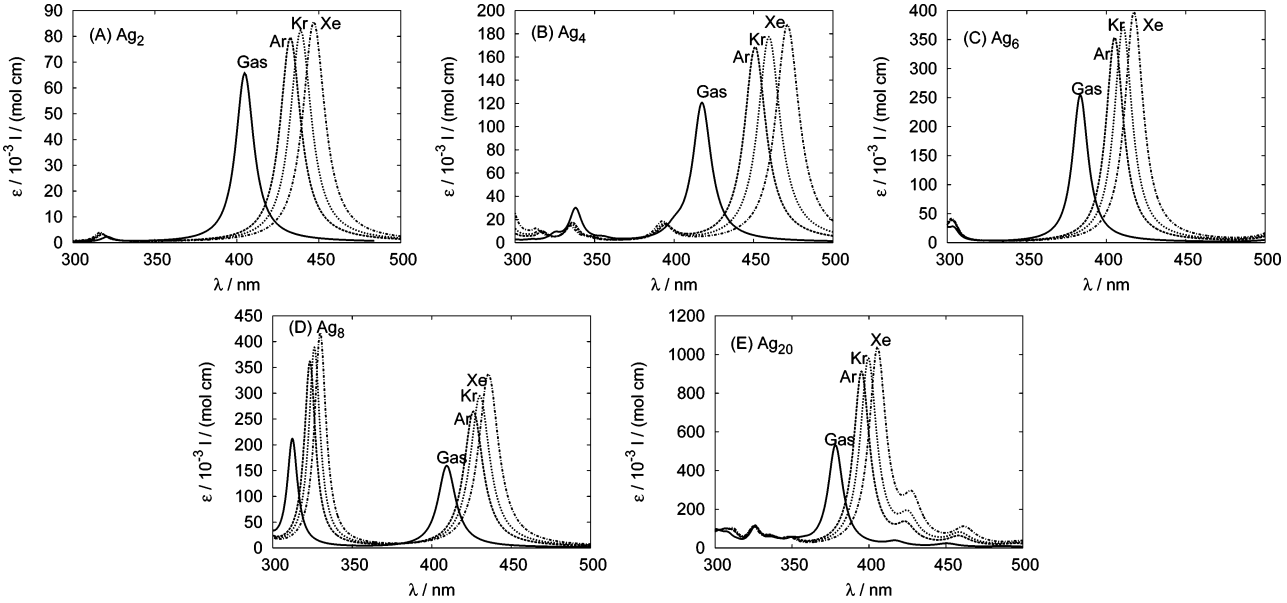

Figure 2. Absorption spectra of Ag_n ($n = 2-8$, 20) clusters embedded in rare gas matrices. Gas phase: solid line; Ar matrix: dashed line; Kr matrix: dotted line; Xe matrix: dot-dashed line. Molar absorption coefficient in units of 10^{-3} L mol^{-1} cm^{-1} and wavelength in nm. Spectra have been broadened by a Lorentzian having a width of 0.1 eV.

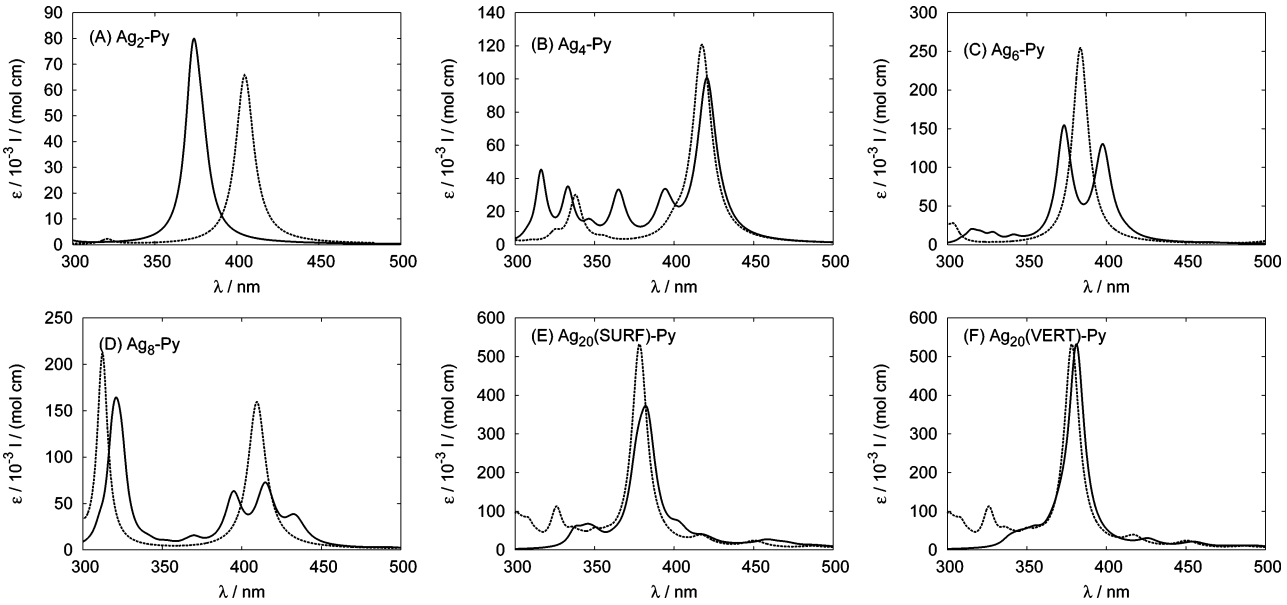

Figure 3. Absorption spectra of Ag_n-Py complexes in the gas phase. Ag_n-Py complexes: solid line; Ag_n clusters: dashed line ($n = 2-8$, 20). Molar absorption coefficient in units of 10^{-3} L mol^{-1} cm^{-1} and wavelength in nm. Spectra have been broadened by a Lorentzian having a width of 0.1 eV.

collected in Figure 2. We see that for all the clusters, in going from the gas phase to Ar, Kr, and Xe matrices, the absorption intensity increases and the absorption maximum shifts to the red. The average shift caused by the Ar matrix is around 0.17 eV, which is in reasonable agreement with the experimental value of 0.24 eV estimated by Buttet et al.[34] The average shift is about 0.06 eV for Xe → Kr and 0.09 eV for Xe → Ar, which, however, are rather small compared with the experimental values of 0.13 eV for the former and 0.22 eV for the latter.[34] Although the COSMO model must be considered a crude model for the rare gas matrices, it seems to provide reasonable solvent shifts for the Ar matrix. However, the model is completely unable to describe the average shift between the different matrices. This could be because the present COSMO implementation neglects all nonelectrostatic effects[66] which are likely to be important, especially for the heavier rare gases. While the present implementation could be extended to include some of these effects, another possibility would be to explicitly include rare gas atoms in the calculations or to adopt a more refined embedding model.[67] However, we will not pursue this since there is already a fair agreement with the experimental results, at least within the expected accuracy of TD-DFT. Note also that COSMO is a continuum model, so as a result, our calculations are able to account for peak red-shifting but not line shape broadening.

Figure 3 presents the simulated absorption spectra of different Ag_n-Py ($n = 2-8$, 20) complexes in the gas phase. We see that except for the Ag_2-Py complex, the absorption maxima of the complexes red-shift a bit compared to those of the corresponding isolated clusters. Adsorption of pyridine leads to symmetry lowering of the clusters, and as a result, we see splitting of the absorption band for the complexes compared to the isolated clusters. The energy splitting is particularly clear for the Ag_6 and Ag_8 clusters, where the single peak around 400

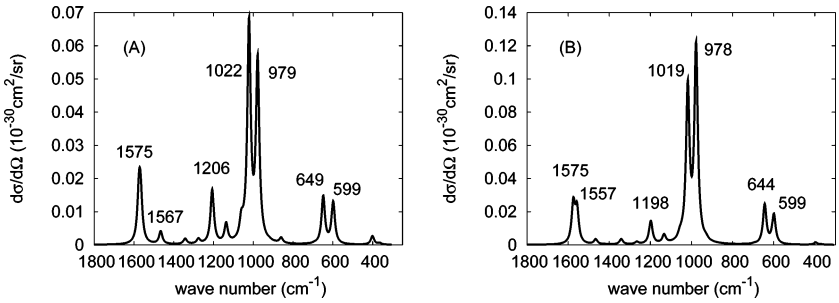

Figure 4. Normal Raman spectra of pyridine in (A) the gas phase and (B) aqueous solution at an incident wavelength of 514.5 nm based on static polarizability derivatives. Differential cross section in units 10^{-30} cm^2/sr and wavenumber in cm^{-1}. Spectra have been broadened by a Lorentzian having a width of 20 cm^{-1}.

nm splits into two or three peaks. Similar to what we found previously without relativistic correction,[26] the shift of the adsorption maximum of the Ag_{20}−Py (SURF) complex is larger than that of the Ag_{20}−Py (VERT) complex, due to stronger orbital interactions.

Interactions between pyridine and the Ag_n clusters also lead to new states which correspond to excitations from the Ag_n cluster to the pyridine molecule. These new charge-transfer (CT) states lie rather low in energy and have very small oscillator strengths. Except for the Ag_4−Py and Ag_{20}−Py (SURF) complexes, these CT states correspond to the lowest metal → molecule excitations. The reason for this is that the interactions destabilize the silver orbitals while at the same time stabilize the pyridine orbitals. CT excitations of pyridine absorbed on a Ag(111) surface have been observed by electron energy loss (EELS) experiments to be around 1.4−2.4 eV.[68] However, it has been proposed that EELS is not suitable for observing such weak CT excitations.[69] In fact, by inverse photoemission (IPE) the unresolved LUMO and LUMO+1 are found to be around 2.9 ± 0.2 eV above the Fermi level.[70] For pyridine on a Cu(111) surface Wolf and co-workers found the states to be at 3.15 and 3.75 eV above the Fermi level using two-photon photoemission (2PPE).[71] Both of these results are significantly higher than the EELS results.

C. Raman Scattering Spectra. In this subsection, we present simulated normal and resonance enhanced Raman scattering spectra of the pyridine molecule and Ag_n−Py (n = 2−8, 20) complexes. Solvent effects are not included in the simulated Raman spectra of the complexes. As mentioned in the Introduction, chemical interaction between molecule and silver cluster, excitation of molecular electronic transitions, excitation of cluster−molecule CT transitions, and excitation of cluster electronic transitions can all lead to enhancement of Raman intensities of the adsorbed molecule. We found previously that the CT enhancements were rather small due to the small oscillator strengths for the CT transitions.[26] Since all of the CT transitions found for the Ag_n−Py complexes are rather weak, and the lowest electronic excitations of pyridine are well-separated from the silver clusters, in the following, we only consider the static chemical and electromagnetic enhancement mechanisms. The enhancement in the normal Raman scattering (NRS) cross section relative to that for pyridine in the absence of the cluster provides a direct measure of the static chemical enhancement, while the cross section at the metal resonance wavelength (a quantity that we refer to as the surface enhanced Raman, or "SERS", cross section) provides an estimate of the combined chemical and electromagnetic enhancements.

One should realize here that the clusters studied are too small to have a real plasmon resonance that involves a collective excitation of all of the conduction electrons. Instead the electronic excitations are molecular in character. However, the excited state can still give rise to the same type of enhancement effects that are familiar from SERS, so we use the same notation. Note also that the detailed decomposition in enhancement mechanisms that we are using would be further complicated if the molecule has electronic transitions which overlap the metal excitations, but this does not happen in the present case. A good example where such overlap occurs is rhodamine 6G (R6G), which is a typical chromophore in single-molecule SERS. We have shown recently that R6G, which has a strong absorption around 530 nm that overlaps with the plasmon resonance in colloidal silver nanoparticles, shows a strong molecular resonance enhancement of 10^5.[43]

The simulated NRS spectra of pyridine (in the absence of a metal cluster) in the gas phase and aqueous solution are presented in Figure 4. The polarizability derivatives needed in eq 1 were calculated at zero frequency; however, a wavelength of 514.5 nm was assumed for the calculations of the differential cross section. Both spectra have then been broadened by a Lorentzian having a width of 20 cm^{-1}.

Note that in our previous works[25−27,43] we used a conversion factor between the scattering factor and the differential cross section in eq 1 that was too large by a factor of 4.5. This affects the absolute intensities but not the relative enhancements and therefore not the conclusions presented. Therefore, the Raman intensities presented here and those published previously differ by a factor of 4.5; however, the appearances of both spectra are the same. The solution spectrum has been calculated by using the implemented COSMO approach in ADF, which accounts for the extra solution (but not local field factors) contribution to the Raman intensities. We see that both simulated spectra are dominated by the two intense ring-breathing modes at ∼1020 and ∼978 cm^{-1}, although the relative intensity of these two peaks is different. Comparing parts B and A of Figure 4, we see that due to inclusion of the solvent effect, the absolute intensities of these two modes are increased much more (almost twice) compared to those of the weaker bands. Although the appearance of the solution-phase spectrum is in better agreement with the experimental results,[72,73] we have found previously that the relative intensities of the two modes at 978 ad 1020 cm^{-1} are sensitive to the choice of exchange functional and basis set,[26] and thus the agreement is somewhat fortuitous.

The simulated NRS and "SERS" spectra of the Ag_n−Py complexes (n = 2−8, 20) are presented in Figure 5. For all the NRS spectra, similar to that of pyridine, the polarizability derivatives needed in eq 1 were calculated at zero frequency; however, a wavelength of 514.5 nm was assumed for the calculations of the differential cross section. For all "SERS" spectra, both polarizability derivatives and differential cross sections were calculated at a wavelength corresponding to one of the absorption maxima of each Ag_n−Py (n = 2−8, 20) complex. The wavelengths used to calculate the "SERS" spectra

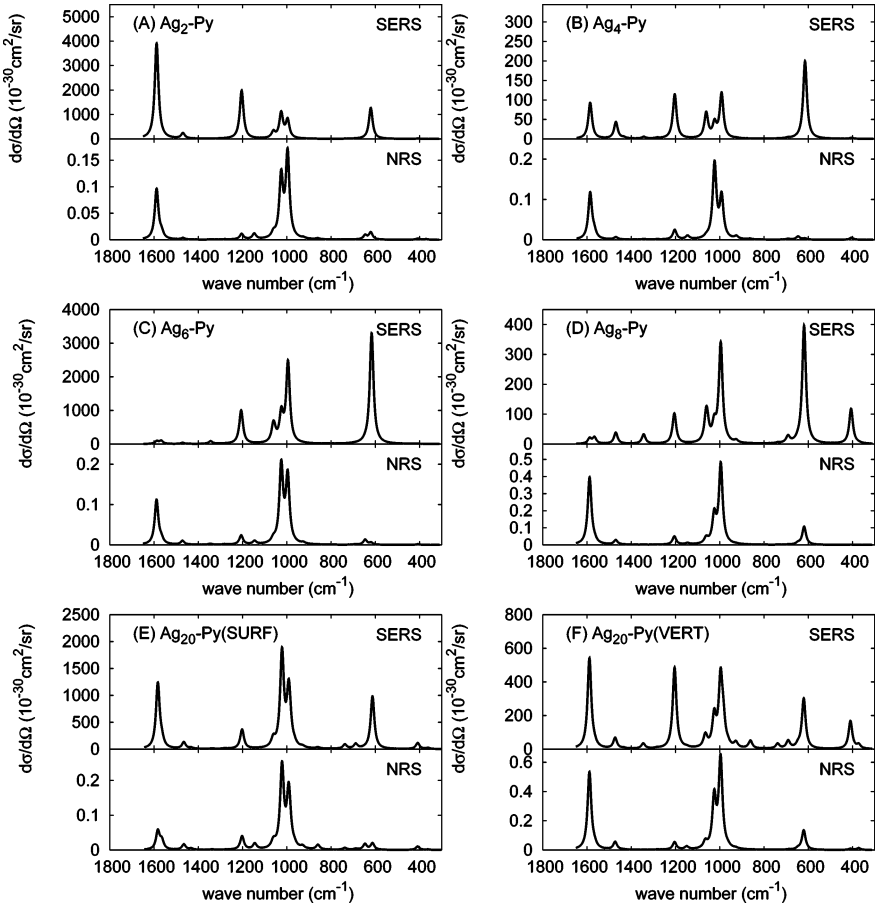

Figure 5. NRS and "SERS" spectra of Ag_n-Py complexes ($n = 2-8$, 20). Differential cross section in units 10^{-30} cm^2/sr and wavenumber in cm^{-1}. Spectra have been broadened by a Lorentzian having a width of 20 cm^{-1}.

TABLE 3: Shifts in Harmonic Frequency (in cm^{-1}), NRS, and "SERS" Enhancement Factor (EF) for Different Ag_n-Py Complexes ($n = 2-8$, 20)

pyridine		av	598.7	648.7	978.6	1022.0	1206.8	1574.5
Ag_2-Py	$\Delta\nu$	8.7	22.0	−2.5	18.0	3.6	−2.6	14.0
	EF_{NRS}	2.3	1.1	0.6	3.1	1.8	0.6	6.5
	EF_{SERS}	23161.1	29070.5	10.4	3846.3	4264.1	32216.6	69558.6
Ag_4-Py	$\Delta\nu$	6.2	16.1	−2.2	13.4	1.7	−3.1	11.3
	EF_{NRS}	2.5	0.3	0.6	2.0	2.9	1.5	7.9
	EF_{SERS}	2328.7	7153.8	1.2	946.0	240.0	2977.4	2653.7
Ag_6-Py	$\Delta\nu$	8.8	20.7	−2.5	17.8	3.3	−0.4	14.2
	EF_{NRS}	2.7	0.4	0.9	3.2	3.0	1.4	7.6
	EF_{SERS}	17637.0	72838.6	409.0	12070.5	3328.3	15781.4	1394.2
Ag_8-Py	$\Delta\nu$	8.5	20.1	−1.9	17.1	3.2	−1.3	13.8
	EF_{NRS}	8.5	8.8	0.7	9.1	2.5	3.0	27.1
	EF_{SERS}	2656.2	11006.3	107.5	2114.3	282.4	2030.6	396.2
$Ag_{20}-Py$ (SURF)	$\Delta\nu$	4.9	14.2	−1.7	13.3	−0.3	−4.5	8.4
	EF_{NRS}	2.5	1.5	1.1	2.9	3.6	2.4	3.6
	EF_{SERS}	11095.3	23787.7	86.2	5274.7	7840.5	6299.0	23283.9
$Ag_{20}-Py$ (VERT)	$\Delta\nu$	8.9	22.0	−2.1	18.0	3.2	−2.4	14.6
	EF_{NRS}	11.5	11.2	0.7	11.9	5.3	3.2	36.5
	EF_{SERS}	4871.0	7259.1	369.3	2228.7	805.4	8369.8	10193.6

are 376, 421, 373, 395, 382, and 383 nm for the Ag_2, Ag_4, Ag_6, Ag_8, Ag_{20} (VERT), and Ag_{20} (SURF) clusters, respectively. The wavelengths were chosen as the strongest transition in the region from 350 to 450 nm.

Note that for the two $Ag_{20}-Py$ complexes, the difference between results presented here and those published in ref 26 is partly due to the wrong conversion factor (a factor of 4.5), and partly due to the inclusion of relativistic effects. Shifts in harmonic frequency and NRS and "SERS" enhancement factors for selected normal modes of pyridine are listed in Table 3. Both the NRS and "SERS" enhancements have been calculated as the ratio of the scattering factors of the complexes over that of the isolated pyridine molecule. The reason why we use the scattering factors here, instead of the differential cross sections as in our previous work,[26,27] when describing the enhancements is to differentiate the dependence on excitation wavelength from the dependence on silver cluster size.

Comparing the NRS spectra in Figure 5 with that of pyridine in Figure 4A, we see that the Raman intensities in the NRS spectrum increase as the cluster size increases, except for the $Ag_{20}-Py$ (SURF) complex. The appearances of these spectra are overall quite similar to the NRS spectrum of pyridine, and the average NRS enhancement is between a factor of 2.3 and 11.5. We found previously[27] that, not surprisingly, the NRS

TABLE 4: Induced Static Polarizability, Imaginary Polarizability, the Distance between the N Atom in Pyridine and the Center of the Metal Cluster, and the Normalized $\alpha^4_{reso}/R^9_{eff}$ Ratio[a]

	$\Delta\bar{\alpha}$	α_{reso}	R_{eff}	$\alpha^4_{reso}/(3R^9_{eff})$	EF_{SERS}/EF_{NRS}
Ag_2-Py	6	1608.6	3.55	12023	10070
Ag_4-Py	15.4	1980.5	4.83	1729	932
Ag_6-Py	15.18	2672.4	5.46	1902	6532
Ag_8-Py	21.5	1050.6	5.19	72	312
$Ag_{20}-Py$ (VERT)	35.5	3399.6	7.43	311	424
$Ag_{20}-Py$ (SURF)	14.0	2521.5	4.70	5809	4438

[a] $\Delta\bar{\alpha} = \bar{\alpha}(Ag_n-Py) - \bar{\alpha}(Ag_n) - \bar{\alpha}(Py)$ is the induced static polarizability (in au). α_{reso} is the imaginary polarizability at resonance calculated from a two-state approximations as $\alpha_{reso} = \mu^2/\Gamma$ where μ is the transition dipole moment and Γ is the damping factor. R_{eff} is the distance between the N atom in pyridine and the center of the metal cluster in Å. The ratio $\alpha^4_{reso}/R^9_{eff}$ has been normalized with a factor of 3 Å to make it numerically similar to the ratio EF_{SERS}/EF_{NRS}.

enhancements correlate quite well with the induced polarizability (i.e., the difference in the polarizability of the complex and the isolated silver cluster and the molecule). The induced polarizabilities of the different complexes are collected in Table 4. We see that indeed there is a good agreement between the size of the NRS enhancement factors and the induced polarizability for all the clusters studied, in agreement with our previous results. The reason for this is that the polarizability is very sensitive to the electronic structure of the system and, therefore, the induced polarizability reflects to what degree the electronic structure of the two systems interacts.

For all complexes, shifts in the harmonic frequencies are observed, with the largest shift for modes at 598, 978, and 1575 cm^{-1}. The ring-stretching mode at 1575 cm^{-1} is enhanced the most for all the complexes considered here. The ring-breathing modes at 978 and 1022 cm^{-1} are also enhanced much more compared to the rest of modes, and the relative importance of these two modes is interchangeable for different sizes of the silver cluster. These results are in agreement with what we found previously for the two $Ag_{20}-Py$ complexes without relativistic effects, and the preference for enhancement of these modes can be understood by considering their vibrational motions (see ref 26 for more details).

Comparing the "SERS" spectra in Figure 5 with Figure 4A, we see that excitation of the silver cluster leads to some quite significant changes. Both the enhancement and the appearance of the Raman spectrum depend strongly on the size of the silver cluster; however, no simple correspondence with cluster size can be found. This is similar to the strong size-dependence that has been found for the polarizability and absorption spectra of small metal clusters.[4,10−13] For these small metal clusters the electronic properties and geometries change dramatically as each new atom is added and one can therefore expect quite different interactions with an adsorbate. This indicates that the use of small clusters in modeling SERS spectra (as has often been done[74−79]) is subject to significant sensitivity to choice of cluster. However, such a strong dependence is only expected for very small clusters.

The total enhancements for all complexes are between 10^3 and 10^4, with the Ag_2-Py complex showing the largest enhancement (Table 3). At first sight these results are quite surprising since one would probably have expected the largest electromagnetic enhancement from the largest cluster due to stronger absorption (see Figure 3). However, what is important is the actual enhanced local field at the location of the molecule, since the electric field decays as $\sim 1/R^3$. For a large particle, changes in the distance on the order of an angstrom are not that important since the molecule is already far from the center of the particle. For a small cluster even small changes in the distance are important since the molecule is so close to the center of the cluster. In the simplest picture the electromagnetic enhancement is expected to scale roughly as $|E^{loc}|^4$. Assuming a point dipole model to calculate the local field would lead to enhancements which scale as $|E^{loc}|^4 \approx \alpha^4_{reso}/R^{12}$. In reality one would expect the electric field to fall off less rapidly than R^{-3} due to deviation from a point dipole model for geometries corresponding to molecular adsorption directly on the particle surface. In Table 4 we have listed for the different complexes the imaginary polarizability at resonance assuming a two-state approximation and the distances, R_{eff}, from the N atom to the center of the clusters. Here it is the imaginary part of the polarizability that is of interest, since in the two-state approximation, the resonance polarizability is purely imaginary and is given by $\alpha_{reso} = i\,\mu^2/\Gamma$, where μ is the transition dipole moment and Γ is the damping factor.[24] Note that the two-state approximation is not used for calculating the Raman spectra. Trial and error leads to the best correlation between the SERS/NRS enhancement ratio and $\alpha^4_{reso}/R^9_{eff}$, which is suggestive of a dipole field enhancement in which the effective field varies as $R^{-2.25}$ rather than R^{-3}. This calculated electromagnetic field enhancement is listed in Table 4 together with the ratio of "SERS" enhancement to "NRS" enhancements. Although there is a reasonable correlation between the two ratios, both with respect to magnitude and the trend, one should realize that this is only a very crude comparison and is not expected to perfectly reflect the complicated enhancements found. Furthermore, for the Ag_{20} clusters there are many transitions located quite close in energy to the wavelengths used in the calculations and their contribution would not be included in the two-state resonant polarizability. However, the reasonable agreement indicates that the enhancement mechanism for these small clusters indeed is similar to the electromagnetic mechanism found for larger nanoparticles.

The enhancements for the Ag_{20} are slightly smaller than was obtained in our previous study,[26] mainly because relativistic effects that are now included in the calculations reduce the oscillator strengths of the silver transitions. For almost all Ag_n-Py complexes, the totally symmetric modes at 598, 978, 1022, 1204, and 1575 cm^{-1} are still enhanced more than the rest; however, more modes are noticeable in the "SERS" spectra compared to the NRS spectra. Compared with experimental SERS spectra (for much larger silver particles),[72] we see that the Ag_{20} cluster is the best model system. In addition, as previously found,[26] the simulated SERS spectrum of the $Ag_{20}-Py$ (SURF) complex is in better agreement with experimental results than that of the VERT complex.

Although we find significant "surface" enhanced Raman scattering for pyridine interacting with the small silver clusters, the enhancements are far from what is needed for single molecule SERS measurements. In contrast to the work by Dickson et al.,[17] which suggested single-molecule Raman scattering for nanometer size or smaller silver particles, we find enhancements that are similar to those for non-single molecule measurements or for molecular resonance Raman scattering. As shown previously[25] our enhancements depend strongly on the value of the damping parameter, Γ. The value we have used leads to reasonable correspondence with the widths observed in matrix isolation spectra (which, however, could be subject to inhomogeneous broadening) and they match the known plasmon width of larger silver particles. However, even if we

adopt a damping factor an order of magnitude smaller (corresponding to a value that is smaller than is commonly used to model resonance Raman spectra of small molecules[41,42]), it would still only lead to enhancements of 10^8. A more quantitative comparison with the scaffold encapsulated silver clusters studied by Dickson et al.[17] is not possible, as the nanoparticle structures in those experiments are not known.

IV. Conclusions

In this work we have presented a TDDFT study of the size-dependence of the absorption and Raman scattering properties of pyridine interacting with small silver nanoclusters Ag_n ($n = 2-8$, 20). Both the normal and "surface"-enhanced Raman spectra have been studied by employing a recently developed short-time approximation for the Raman scattering cross section. The absorption spectra of the small silver clusters have been studied both in the gas phase and embedded in rare gas matrices to model the experimental conditions. The rare gas matrices have been modeled by a nonequilibrium COSMO model and the absorption spectra are found to be in reasonable agreement with the available experimental results and other theoretical studies. The results show that both the absorption and Raman properties depend strongly on cluster size and adsorption site. The NRS spectra of the Ag_n−pyridine complexes appear quite similar to the NRS spectrum of pyridine, with average enhancements that increase slowly with cluster size but are always below a factor of 12. However, for the SERS spectra the situation is quite different. Both the enhancement and the appearance of the Raman spectra show a very strong dependence on cluster size. The total enhancements for the complexes are between 10^3 and 10^4 and quite surprisingly the strongest enhancement is found for the Ag_2−Py complex. However, the enhancement trends can be correlated with the distance of the molecule to the center of the metal cluster and the polarizability at resonance. This indicates that that enhancement mechanism for the small clusters is similar to the electromagnetic mechanism for larger nanoparticles.

Acknowledgment. L.J., L.L.Z., and G.C.S. thank the Air Force Office of Scientific Research MURI program (F49620-02-1-0381) and DOD DURINT (F49620-01-1-0401). We were also supported by the U.S. Department of Energy under grant DEFGOZ-03-ER15487. This research was performed in part with use of the Molecular Science Computing Facility (MSCF) in the William R. Wiley Environmental Molecular Sciences Laboratory, a national scientific user facility sponsored by the U.S. Department of Energy's Office of Biological and Environmental Research and located at the Pacific Northwest National Laboratory, operated for the Department of Energy by Battelle.

References and Notes

(1) Moskovits, M. *Rev. Mod. Phys.* **1985**, *57*, 783−826.
(2) Campion, A.; Kambhampati, P. *Chem. Soc. Rev.* **1998**, *27*, 241−250.
(3) Kneipp, K.; Kneipp, H.; Itzkan, I.; Dasari, R. R.; Feld, M. S. *Chem. Rev.* **1999**, *99*, 2957−2975.
(4) Link, S.; El-Sayed, M. A. *Annu. Rev. Phys. Chem.* **2003**, *54*, 331.
(5) Mirkin, C. A.; Letsinger, R. L.; Mucic, R. C.; Storhoff, J. J. *Nature* **1996**, *382*, 607−609.
(6) Haes, A. J.; Hall, W. P.; Chang, L.; Klein, W. L.; Van, Duyne, R. P. *Nano Lett.* **2004**, *4*, 1029−1034.
(7) Yonzon, C. R.; Haynes, C. L.; Zhang, X.; Walsh, J. T., Jr.; Van Duyne, R. P. *Anal. Chem.* **2004**, *76*, 78−85.
(8) Wood, D. M.; Ashcroft, N. W. *Phys. Rev. B* **1982**, *25*, 6255.
(9) Liebsch, A. *Phys. Rev. B* **1993**, *48*, 11317.
(10) de Heer, W. A. *Rev. Mod. Phys.* **1993**, *65*, *611*.
(11) Halperin, W. P. *Rev. Mod. Phys.* **1986**, *58*, *533*.
(12) Bonačić-Koutecký, V.; Fantucci, P.; Koutecký, J. *Chem. Rev.* **1991**, *91*, 1035.
(13) Brack, M. *Rev. Mod. Phys.* **1993**, *65*, 677.
(14) Haslett, T. L.; Bosnick, K. A.; Moskovits, M. *J. Chem. Phys.* **1998**, *108*, 3453−3457.
(15) Haslett, T. L.; Bosnick, K. A.; Fedrigo, S.; Moskovits, M. *J. Chem. Phys.* **1999**, *111*, 6456−6461.
(16) Bosnick, K. A.; Haslett, T. L.; Fedrigo, S.; Moskovits, M. *J. Chem. Phys.* **1999**, *111*, 8867−8870.
(17) Peyser-Capadona, L.; Zheng, J.; Gonzalez, J. I.; Lee, T.-H.; Patel, S. A.; Dickson, R. M. *Phys. Rev. Lett.* **2005**, *94*, 058301(1)−058301(4).
(18) Nie, S. M.; Emory, S. R. *Science* **1997**, *275*, 1102−1106.
(19) Michaels, A. M.; Nirmal, M.; Brus, L. E. *J. Am. Chem. Soc.* **1999**, *121*, 9932−9939.
(20) Kneipp, K.; Wang, Y.; Kneipp, H.; Perelman, L. T.; Itzkan, I.; Dasari, R. R.; Feld, M. S. *Phys. Rev. Lett.* **1997**, *78*, 1667−1670.
(21) Xu, H.; Bjerneld, E. J.; Käll, M.; Börjesson, L. *Phys. Rev. Lett.* **1999**, *83*, 4357−4360.
(22) Otto, A. Surface enhanced Raman scattering: "classical" and "chemical" origins. In *Topics of Applied Physics 54*; Light Scattering in Solids, Vol. IV; Cardona, M., G. G., Eds.; Springer: Secaucus, NJ, 1984.
(23) Schatz, G. C.; Van Duyne, R. P. Electromagnetic mechanism of surface enhanced spectroscopy. In *Handbook of Vibrational Spectroscopy*; Chalmers, J. M., Griffiths, P. R., Eds.; John Wiley and Sons, Ltd: New York, 2002; Vol. 1.
(24) Jensen, L.; Autschbach, J.; Schatz, G. C. *J. Chem. Phys.* **2005**, *122*, 224115.
(25) Jensen, L.; Zhao, L. L.; Autschbach, J.; Schatz, G. C. J. *Chem. Phys.* **2005**, *123*, 174110(1)−174110(11).
(26) Zhao, L. L.; Jensen, L.; Schatz, G. C. *J. Am. Chem. Soc.* **2006**, *128*, 2911−2919.
(27) Zhao, L. L.; Jensen, L.; Schatz, G. C. *Nano Lett.* **2006**, *6*, 1229−1234.
(28) Fedrigo, S.; Harbich, W.; Buttet, J. *J. Chem. Phys.* **1993**, *99*, 5712−5717.
(29) Félix, C.; Sieber, C.; Harbich, W.; Buttet, J.; Rabin, I.; Schulze, W.; Ertl, G. *Phys. Rev. Lett.* **2001**, *86*, 2992−2995.
(30) Harbich, W.; Fedrigo, S.; Meyer, F.; Lindsay, D. M.; Lignieres, J.; Rivoal, J. C.; Kreisle, D. *J. Chem. Phys.* **1990**, *93*, 8535−8543.
(31) Félix, C.; Sieber, C.; Harbich, W.; Buttet, J.; Rabin, I.; Schulze, W.; Ertl, G. *Chem. Phys. Lett.* **1999**, *313*, 105−109.
(32) Rabin, I.; Schulze, W.; Ertl, G. *J. Chem. Phys.* **1998**, *108*, 5137−5142.
(33) Konig, L.; Rabin, I.; Schulze, W.; Ertl, G. *Science* **1996**, *274*, 1353−1354.
(34) Fredigo, S.; Harbich, W.; Buttet, J. *Phys. Rev. B* **1993**, *47*, 10706−10715.
(35) Klamt, A.; Schüürmann, G. *J. Chem. Soc., Perkin Trans. 2* **1993**, 799−805.
(36) Pye, C. C.; Ziegler, T. *Theor. Chim. Acta* **1999**, *101*, 396−407.
(37) Jensen, L.; Schatz, G. C. Unpublished.
(38) Neugebauer, J.; Reiher, M.; Kind, C.; Hess, B. A. *J. Comput. Chem.* **2002**, *23*, 895−910.
(39) Boyd, R. W. *Nonlinear Optics*; Academic Press: San Diego, CA, 1992.
(40) Schatz, G. C.; Ratner, M. A. *Quantum Mechanics in Chemistry*; Dover: New York, 2002.
(41) Sue, J.; Yan, Y. J.; Mukamel, S. *J. Chem. Phys.* **1986**, *85*, 462−474.
(42) Meyers, A. B. *Annu. Rev. Phys. Chem.* **1998**, *49*, 267−295.
(43) Jensen, L.; Schatz, G. C. *J. Phys. Chem. A* **2006**, *110*, 5973−5977.
(44) Baerends, E. J.; Autschbach, J.; Bérces, A.; Bo, C.; Boerrigter, P. M.; Cavallo, L.; Chong, D. P.; Deng, L.; Dickson, R. M.; Ellis, D. E.; et al. "ADF", http://www.scm.com, 2005.
(45) te Velde, G.; Bickelhaupt, F. M.; Baerends, E. J.; Fonseca Guerra, C.; van Gisbergen, S. J. A.; Snijders, J. G.; Ziegler, T. *J. Comput. Chem.* **2001**, *22*, 931.
(46) Becke, A. D. *Phys. Rev. A* **1988**, *38*, 3098.
(47) Perdew, J. P. *Phys. Rev. B* **1986**, *33*, 8822.
(48) van Lenthe, E.; Baerends, E. J.; Snijders, J. G. *J. Chem. Phys.* **1993**, *99*, 4597−4610.
(49) van Lenthe, E.; Baerends, E. J.; Snijders, J. G. *J. Chem. Phys.* **1994**, *101*, 9783−9792.
(50) Bonačić-Koutecký, V.; Pittner, J.; Boiron, M.; Fantucci, P. *J. Chem. Phys.* **1999**, *110*, 3876−3886.
(51) Bonačić-Koutecký, V.; Veyret, V.; Mitrić, R. *J. Chem. Phys.* **20001**, *115*, 10450−10460.
(52) Yabana, K.; Bertsch, G. F. *Phys. Rev. A* **1999**, *60*, 3809−3814.
(53) Idrobo, J. C.; Öğüt, S.; Jellinek, J. *Phys. Rev. B* **2005**, *72*, 085445-1−085445-11.
(54) Demuth, J. E.; Christmann, K.; Sanda, P. N. *Chem. Phys. Lett.* **1980**, *76*, 201−206.

(55) Bader, M.; Haase, J.; Frank, K.-H.; Puschmann, A.; Otto, A. *Phys. Rev. Lett.* **1986**, *56*, 1921−1924.
(56) Moskovits, M.; DiLella, D. P.; Maynard, K. J. *Langmuir* **1988**, *4*, 67−76.
(57) Lee, J.-G.; Ahner, J.; Yates, J. T., Jr. *J. Chem. Phys.* **2001**, *114*, 1414−1419.
(58) Hahn, J. R.; Ho, W. *J. Chem. Phys.* **2006**, *124*, 204708-1−204708-4.
(59) Jeanmaire, D. L.; Van Duyne, R. P. *J. Electroanal. Chem.* **1974**, *84*, 1−20.
(60) Creighton, J. A.; Albrecht, M. G.; Hester, R. E.; Matthew, J. A. D. *Chem. Phys. Lett.* **1978**, *55*, 55−58.
(61) Krasser, W.; Kettler, U.; Bechthold, P. S. *Chem. Phys. Lett.* **1982**, *86*, 223−227.
(62) Clark, R. J. H.; Williams, C. S. *Inorg. Chem.* **1965**, *4*, 350−357.
(63) Yang, M. C.; Rockey, T. J.; Pursell, D.; Dai, H. L. *J. Phys. Chem. B* **2001**, *105*, 11945−11948.
(64) Fernández, E. M.; Soler, J. M.; Garzón, I. L.; Balbás, L. C. *Phys. Rev. B* **2004**, *70*, 165403(1)−165403(14).
(65) Yang, M.; Jackson, K. A.; Jellinek, J. *J. Chem. Phys.* **2006**, *125*, 144308.
(66) Tomasi, J.; Mennucci, B.; Cammi, R. *Chem. Rev.* **2005**, *105*, 2999−3093.
(67) Gervais, B.; Giglio, E.; Jacquet, E.; Ipatov, A.; Reinhard, P.-G.; Fehrer, F.; Suraus, E. *Phys. Rev. A* **2005**, *71*, 015201-1−015210-4.
(68) Avouris, P.; Demuth, J. E. *J. Chem. Phys.* **1981**, *75*, 4783−4794.
(69) Zylka, G.; Otto, A. *Surf. Sci.* **2001**, *475*, 118−130.
(70) Otto, A.; Frank, K. H.; Reihl, B. *Surf. Sci.* ***1985***, *163*, *140*.
(71) Zhong, Q.; Gahl, C.; Wolf, M. *Surf. Sci.* **2002**, *496*, 21−32.
(72) Golab, J. T.; Sprague, J. R.; Carron, K. T.; Schatz, G. C.; Van Duyne, R. P. *J. Chem. Phys.* **1988**, *88*, 7942−7951.
(73) Klots, T. D. *Spectrochim. Acta, Part A* **1998**, *54*, 1481−1498.
(74) Yang, W.-H.; Schatz, G. C. *J. Chem. Phys.* **1992**, *97*, 3831−3845.
(75) Aroca, R. F.; Clavijo, R. E.; Halls, M. D.; Schlengel, H. B. *J. Phys. Chem. A* **2000**, *104*, 9500−9505.
(76) Cardini, G.; Muniz-Miranda, M. *J. Phys. Chem. B* **2002**, *106*, 6875−6880.
(77) Vivoni, A.; Birke, R. L.; Foucault, R.; Lombardi, J. R. *J. Phys. Chem. B* **2003**, *107*, 5547−5557.
(78) Wu, D. Y.; Hayashi, M.; Lin, S. H.; Tian, Z. Q. *Spectrochim. Acta, Part A* **2004**, *60*, 137−146.
(79) Johansson, P. *Phys. Chem. Chem. Phys.* **2005**, *7*, 475−482.